International Journal of Mass Spectrometry 330–332 (2012) iii–xiii

Contents lists available at ScienceDirect

International Journal of Mass Spectrometry

journal homepage: www.elsevier.com/locate/ijms

Contents

Foreword

1–1

Ion Structures and Energetics, and Ion-Molecule Reaction Kinetics in the Gas Phase. A Collection of Invited Papers Dedicated to Peter B. Armentrout on the Occasion of His 60th Birthday

Mary T. Rodgers, David E. Clemmer

2–3

An Appreciation

Mary T. Rodgers, David E. Clemmer

4–5

A Celebration of the Scientific and Personal Contributions of Peter B. Armentrout

Mary T. Rodgers, David E. Clemmer

Elsevier B.V.
http://dx.doi.org/10.1016/S1387-3806(12)00395-8

Regular Articles

6–15

Infrared multiple photon dissociation spectroscopy of protonated histidine and 4-phenyl imidazole

Murat Citir, Christopher S. Hinton, Jos Oomens, Jeffrey D. Steill, P.B. Armentrout

► Protonated histidine (His) and 4-phenyl imidazole (PhIm) are examined by infrared multiple photon dissociation (IRMPD) action spectroscopy. ► Structures are determined by comparing the spectra with B3LYP/6–311+G(d,p) predictions. ► The dominant structure of H^+(His) has the protonated nitrogen atom of imidazole hydrogen bonding to the backbone amino nitrogen. ► Results are compared to IRMPD studies of protonated histamine, radical $His^{\bullet+}$, H^+(HisArg), H_2^{2+}(HisArg), and M^+(His), where M^+ = alkali cations.

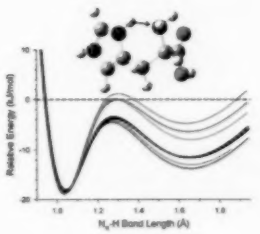

16–26

Alkali metal cation interactions with 12-crown-4 in the gas phase: Revisited

P.B. Armentrout, C.A. Austin, M.T. Rodgers

► Alkali metal cation binding affinities of 12C4 are determined using threshold CID methods. ► Gas phase DC-FT versus ESI formation of M^+(12C4) can produce different structures. ► Ground-state C4 conformers of M^+(12C4) are produced by ESI and by DC-FT for Na^+ and K^+. ► Excited C2 conformers of M^+(12C4) are produced by DC-FT for Rb^+ and Cs^+. ► M^+–12C4 BDEs obtained by TCID and B3LYP/def2-TZVPPD agree very well.

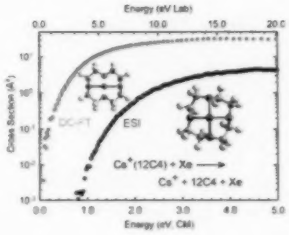

27–34

Alkali metal cation–cyclen complexes: Effects of alkali metal cation size on the structure and binding energy

C.A. Austin, Y. Chen, M.T. Rodgers

► Alkali metal cation binding affinities of cyclen are determined using threshold CID methods. ► Ground-state C4(++++) conformers of M^+(cyclen) are produced by ESI for Na^+, K^+, Rb^+, and Cs^+. ► M^+–cyclen BDEs obtained by TCID and B3LYP/def2-TZVPPD agree very well. ► Cyclen exhibits a strong preference over 12-crown-4 for binding to hard metal cations, e.g. Na^+. ► Cyclen is competitive with, but binds the larger alkali metal cations, K^+, Rb^+, and Cs^+, slightly less strongly than 12-crown-4.

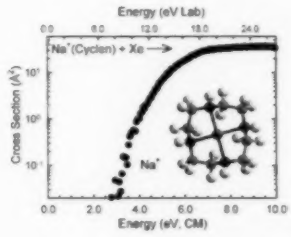

35–45

A database of alkali metal-containing peptide cross sections: Influence of metals on size parameters for specific amino acids

Jonathan M. Dilger, Stephen J. Valentine, Matthew S. Glover, Michael A. Ewing, David E. Clemmer

► The first large database of collision cross sections for metal-containing peptides is reported. ► General trends in the sizes of peptide ions are extracted upon association with alkali cations of increasing size. ► Differences in intrinsic size parameter (ISP) values for alkali-metal cationized peptides as compared to protonated peptides show the influence on cross section of alkali cations with specific amino acid residues.

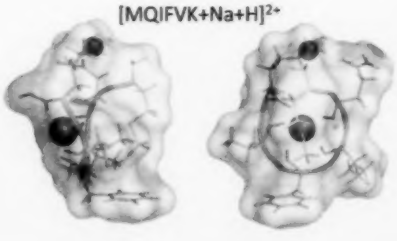

46–57

Ion contributions to gas–surface interactions in inductively-coupled fluorocarbon plasmas

Michael F. Cuddy, Joshua M. Blechle, Ellen R. Fisher

► Nascent ions in fluorocarbon (FC) plasmas were identified and energy analyzed. ► Ion effects are mediated both by plasma parameters and the choice of precursor. ► Highly energetic ions induce CF_x scatter at surfaces. ► Low energy plasma ions recombine in the gas phase to promote FC film growth. ► FC deposition rates are strongly influenced by gas-phase oligomer concentration.

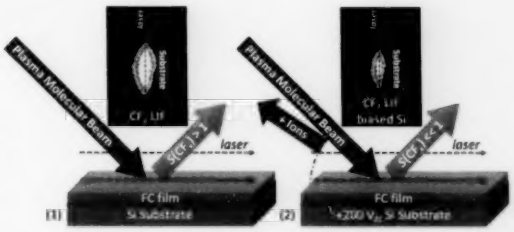

58–62

Metastable fragmentation of photoionized styrene cluster ions: Implications for cluster ion structure

David A. Hales, Kevin L. Kmiec, Catrin M. Mills, Patrick D. Rawhouser, Shawna Rigsby McGehee

► Photoionized styrene cluster ions show intensity alternation in the mass spectrum.
► Metastable fragmentation shows almost exclusively evaporation of whole molecules.
► Fragment ion intensity patterns imply formation of a covalently bound dimer ion.
► Our results do not support but also do not disprove earlier structural predictions.

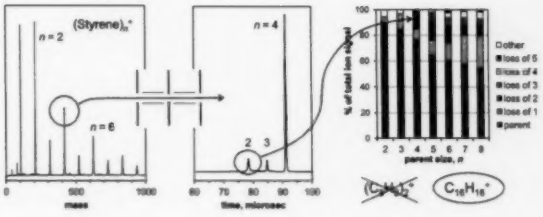

63–70

Theory of the protein equilibrium population snapshot by H/D exchange electrospray ionization mass spectrometry (PEPS-HDX-ESI-MS) method used to obtain protein folding energies/rates and selected supporting experimental evidence

Rohana Liyanage, Nagarjuna Devarapalli, Derek B. Pyland, Latisha M. Puckett, N.H. Phan, Joel A. Starch, Mark R. Okimoto, Jennifer Gidden, Wesley E. Stites, Jackson O. Lay Jr.

► ~1 s HDX PEPS intensities of deuterated closed and open state forms of ubiquitin represents a true "snapshot" of the protein equilibrium. ► Theoretical model which used a two state protein folding mechanism and the "breathing model" of HDX explain how short 1 s HDX PEPS experiments work in estimating protein folding energies. ► PEPS can also be used to estimate protein folding/unfolding rates.

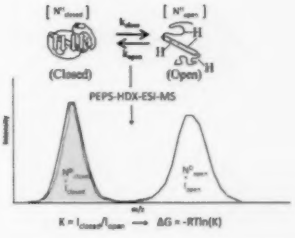

71–77

Metal ion binding to peptides: Oxygen or nitrogen sites?

Robert C. Dunbar, Nicolas C. Polfer, Giel Berden, Jos Oomens

► Gas-phase ion-peptide complex structures as a function of metal and ligand. ► Conformation determination by gas-phase IRMPD spectroscopy. ► Iminol tautomerization of metal-ion-bound peptide ligands. ► Diagnostic application of IR Amide II band for identifying metal-amide-nitrogen bonding. ► Peptide size effect on Mg^{2+} binding conformations.

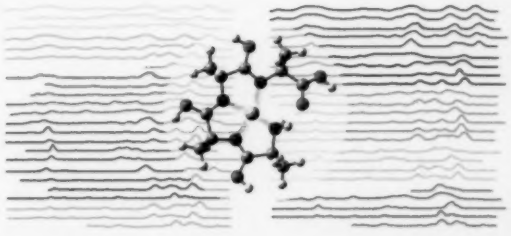

78–84

A novel projection approximation algorithm for the fast and accurate computation of molecular collision cross sections (III): Application to supramolecular coordination-driven assemblies with complex shapes

Stanley E. Anderson, Christian Bleiholder, Erin R. Brocker, Peter J. Stang, Michael T. Bowers

► Supramolecular complexes are investigated by ion mobility mass spectrometry. ► Experimental cross sections are compared to computational cross sections. ► The projected superposition approximation (PSA) provides the best comparison with experiment. ► The shape factor needs a finer mesh for molecules with unusual topographies.

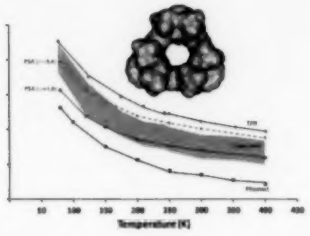

85–94

Spatial extent of fragment-ion abundances in electron transfer dissociation and electron capture dissociation mass spectrometry of peptides

Jack Simons, Aaron R. Ledvina

► Spatial extents of ETD and ECD fragmentation patterns are modeled. ► They seem to mimic the spatial extent of Rydberg orbitals having $n = 3–6$. ► Several sets of ETD and ECD data are analyzed.

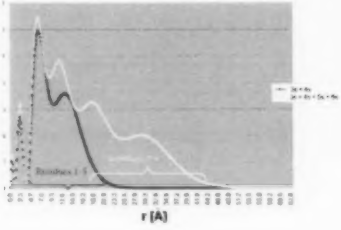

95–99

Ligand effects on single-electron transfer of isolated iron atoms in the gaseous complexes $[(OC)_mFe(OH_2)_n]^+$ ($m, n = 0–2$, $m + n = 1, 2$)

František Karlický, Michal Otyepka, Detlef Schröder

► High level ab *initio* studies of the small neutral and monocationic species $[(OC)_mFe(OH_2)_n]^+$ ($m, n = 0–2$, $m + n = 1, 2$). ► CO as a ligand stabilizes the low-spin configuration in the cationic as well as the neutral forms. ► Carbonyl complexes form bound states for the neutral species. ► Redox chemistry of iron is drastically influenced by ligation.

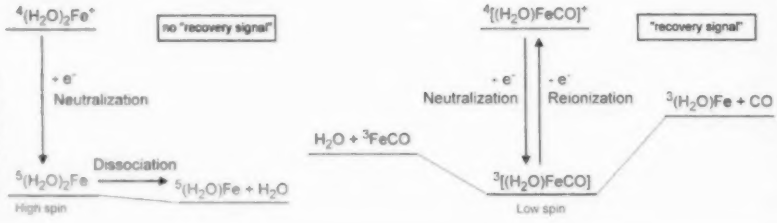

100–108

Dissociating $C_3H_5Br^+$ ions: Almost all roads lead to the allyl cation

Sampada Borkar, Bálint Sztáray, Andras Bodi

► Bromine-loss unimolecular dissociation of internal energy selected $C_3H_5Br^+$ isomer ions was studied by iPEPICO spectroscopy. ► Quantum chemical calculations were used to map out the potential energy surface connecting the various isomer cations. ► 1-Br-propenes, allyl bromide, and Br-cyclopropane form the allyl cation; 2-Br-propene dissociates to the 2-propenyl cation. ► Dissociation of the 1-bromopropene cations starts with isomerization to the allyl bromide cation prior to dissociation. ► A mixed theoretical/experimental thermochemical network was used to determine heats of formation of five C_3H_5Br isomers.

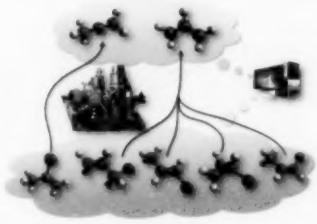

109–117

Synthesis and gas-phase uni- and bi-molecular reactivity of bisphosphine ligated gold clusters, $[Au_xL_y]^{n+}$

Peter S.D. Robinson, Tich-Lam Nguyen, Hadi Lioe, Richard A.J. O'Hair, George N. Khairallah

► Novel bisphosphine protected gold cluster cations $[Au_xLy_n]^{z+}$ (x = 3, 5–11; y = 1–5 and z = 1–3). ► Gas phase ion-molecule reactions using various neutral reagents were used to provide information on possible reactive sites in the clusters. ► The observed lack of reactivity of several of these clusters is consistent with previously determined X-ray structures. ► Gold atoms are not available for reaction when they are capped with phosphine groups.

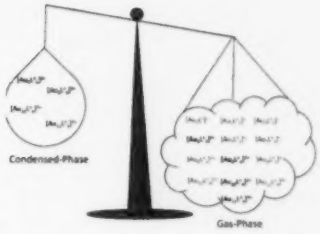

118–123

Gas-phase infrared spectrum of the anionic GFP-chromophore

Mitra Almasian, Josipa Grzetic, Giel Berden, Bert Bakker, Wybren Jan Buma, Jos Oomens

► First gas-phase IR spectrum of the isolated anionic GFP chromophore. ► Good correspondence between experimental and theoretical IR spectra. ► IR spectrum for the main, radical anion fragment of HBDI at m/z 200.

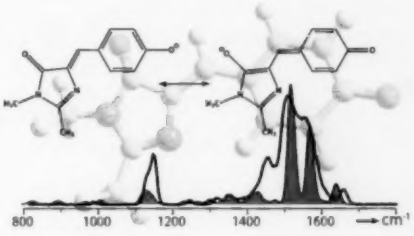

124–133

Fragmentation reactions of thiourea- and urea-compounds examined by tandem MS-, energy-resolved CID experiments, and theory

Francesco Falvo, Lukas Fiebig, Frank Dreiocker, Ran Wang, P.B. Armentrout, Mathias Schäfer

► CID Fragmentation reactions of thiourea- and urea-compounds are investigated in detail. ► QIT-CID MS^n, energy-resolved CID, exact ion mass measurements and theory are applied for the study. ► The combination of independent measurements allows elucidating fragmentation reactions.

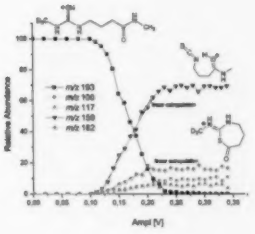

134–143

IRMPD and DFT study of the loss of water from protonated 2-hydroxynicotinic acid

Michael Van Stipdonk, Michael Kullman, Giel Berden, Jos Oomens

► Infrared multiple photon dissociation (IRMPD) spectroscopy and density functional theory (DFT) calculations used to study the elimination of water from protonated 2-hydroxynicotinic acid. IRMPD shows that the product generated by loss of water is an acylium ion with 2-pyridone like structure. ► DFT calculations suggest that loss of water occurs through concerted proton transfer and C—OH bond cleavage through 6 membered ring transition state.

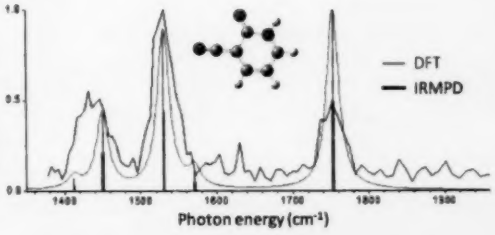

144–151

Effect of phenol and acidic side chains on the protonation sites of b_2 ions confirmed by IRMPD spectroscopy

Da Wang, Kerim Gulyuz, Corey N. Stedwell, Long Yu, Nicolas C. Polfer

► IR spectra were recorded in the hydrogen stretching region for the b_2 ions of YGG, GYG, EGG and GEG. ► In all cases, exclusive presence of oxazolone structures is confirmed. ► Proton attachment at the N-terminus or oxazolone ring N depends on the sequence order. ► The aromatic or acidic side chain can stabilize protonation at the N-terminus.

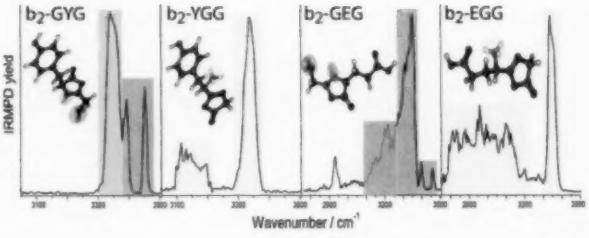

152–159

Electron detachment dissociation of synthetic heparan sulfate glycosaminoglycan tetrasaccharides varying in degree of sulfation and hexuronic acid stereochemistry

Franklin E. Leach III, Sailaja Arungundram, Kanar Al-Mafraji, Andre Venot, Geert-Jan Boons, I. Jonathan Amster

► Application of electron detachment dissociation to increasingly sulfated GAGs. ► Development of a two-step method for sulfation and C5 stereochemistry determination. ► Determination of hexuronic acid stereochemistry in highly sulfated tetrasaccharides. ► Desulfation of sulfated GAG tetrasaccharides to determine C5 stereochemistry.

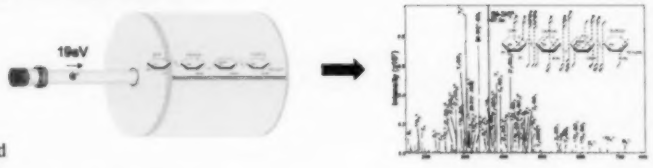

160–167

S-nitrosation of cysteine as evidenced by IRMPD spectroscopy

Francesco Lanucara, Barbara Chiavarino, Maria Elisa Crestoni, Debora Scuderi, Rajeev K. Sinha, Philippe Maître, Simonetta Fornarini

► Protonated and deprotonated S-nitrosocysteine ions are assayed in the gas phase by IRMPD spec-troscopy. ► The ions from S-nitrosocysteine are examined in parallel with the ions from the native amino acid. ► The spectrum of the anion (red) reveals a NO feature in a blank portion of the spectrum of deprotonated cysteine (green). ► DFT calculations underline the presence of several conformers contributing to the overall IR spectrum (black).

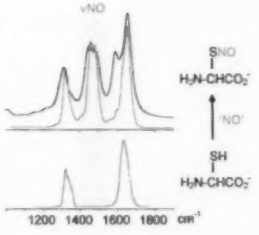

168–173

Dissociation of deprotonated glycine complexes with Pb^{2+} and five transition-metal dications (Fe^{2+}, Co^{2+}, Ni^{2+}, Cu^{2+}, Zn^{2+}): The importance of metal bond activation

Laura Banu, Voislav Blagojevic, Diethard K. Bohme

► We electrosprayed 1:1 complexes of deprotonated glycine (Gly-H)− and the metal dications Fe^{2+}, Co^{2+}, Ni^{2+}, Cu^{2+}, Zn^{2+}, Pb^{2+}. ► These metal complexes and bare (Gly-H)− were exposed to multi-collisional dissociation. ► We discovered trends in the extent of dissociation and the nature of ion products formed. ► This provided insights into the capacity of chemical bond activation by metal dications and dissociation mechanisms. ► The number of electrons in the valence shell of the metal dication appears to be important.

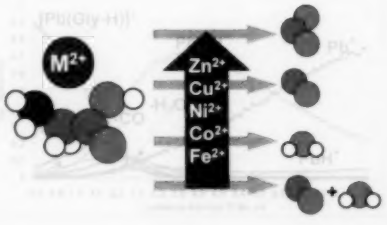

174–181

Electron transfer dissociation: Effects of cation charge state on product partitioning in ion/ion electron transfer to multiply protonated polypeptides

Jian Liu, Scott A. McLuckey

► The z-state dependencies of the competitions between PT versus ET, ETD versus ETnoD, and side-chain cleavage versus backbone cleavage in ETD are described. ► ET increases relative to PT as peptide z-state increases. ► ETD increases relative to ET,noD as peptide z-state increases. ► Back-bone cleavage increases relative to side-chain loss as z-state increases. ► Factors that underlie these trends are discussed.

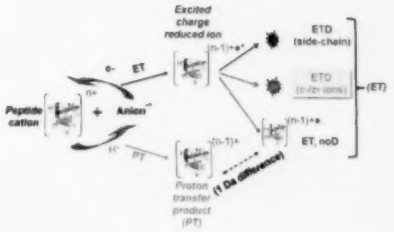

182–190

The α-effect in elimination reactions and competing mechanisms in the gas phase

John M. Garver, Zhibo Yang, Nadine Wehres, Charles M. Nichols, Benjamin B. Worker, Veronica M. Bierbaum

► The intrinsic behavior of α -nucleophiles is explored in the gas phase. ► Reagent pairs must have comparable proton affinities to assess intrinsic differences. ► E2 reactions show similar reactivity for α- and normal anions. ► S_N2 and $B_{AC}2$ mechanisms show enhanced reactivity of α-anions. ► The behavior of α-nucleophiles can be rationalized by "soft" base behavior.

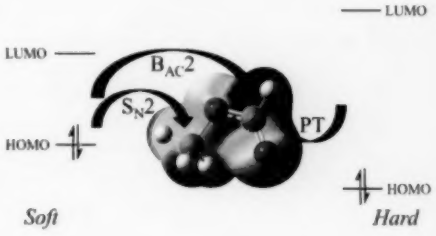

191–199

Proton mobility and stability of water clusters containing alkali metal ions

Alexey Sergeevich Zatula, Mauritz Johan Ryding, Patrik Urban Andersson, Einar Uggerud

► Abundance mass spectra of $M^+(H_2O)_n$ (M = Li, Na, K, Rb and Cs) have been recorded. ► Magic number peaks in abundance spectra and in evaporation spectra are identical. ► Reactions with D_2O show that proton mobility is insignificant in all $M^+(H_2O)n$. ► Quantum chemical calculations show that activation energies for H/D exchange are high. ► These clusters will be useful for benchmarking in future studies of H/D exchange.

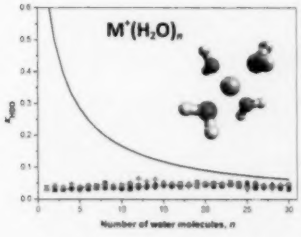

200–206

Gas-phase hydrogen deuterium exchange behavior of lysine and its homologs

Justine V. Arrington, Rita N. Straus, Patrick F. Reynolds, Jennifer L. Poutsma, Elaine M. Marzluff, John C. Poutsma

► We determined HDX rate coefficients for lysine its three lower homologs. ► All four homologs exchange all six labile hydrogens for deuterium using D_2O. ► The data are consistent with relay and flip–flop mechanisms. ► DapaH⁺ exchanges the fastest, LysH⁺ and DabaH⁺ are slower, and OrnH⁺ is 30–50 times slower. ► The exchange rates correlate with calculated HDX barriers at the B3LYP/6- 31+G(d,p) level.

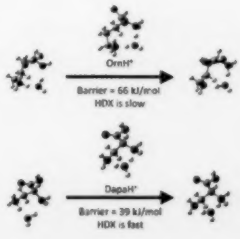

207–219

Correlating ETD fragment ion intensities with peptide ion conformational and electronic structure

František Tureček, Christopher L. Moss, Thomas W. Chung

► We identified most stable conformers of gas-phase $(AAXAR + 2H)^{2+}$ peptide ions. ► Electron attachment to $(AAXAR + 2H)^{2+}$ forms zwitterionic cation-radicals. ► Backbone cleavage occurs near the protonated (Arg) or polar (His, Asp) residues. ► Proton migration from neutral amide groups is disfavored. ► The chicken-and-egg problem of the ExD dissociation mechanism is addressed.

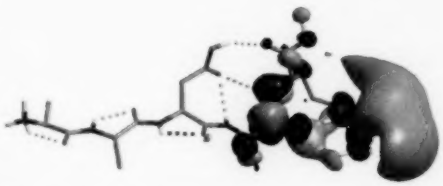

C electronic state of $(AADAR + 2H)^{+\bullet}$

220–225

Protein structure evolution in liquid DESI as revealed by selective noncovalent adduct protein probing

Benjamin N. Moore, Omar Hamdy, Ryan R. Julian

► Protein structure retention in liquid DESI examined. ► Mechanisms of ESI and liquid DESI compared. ► Liquid DESI is well suited for SNAPP. ► Structures of natively disordered proteins probed.

226–232

Silver(I) and gold(I) complexes of diethylmalonate

Anton Škríba, Lucie Jašíková, Jana Roithová

► Complexes of diethylmalonate with silver(I) and gold(I) cations were investigated using IRMPD spectroscopy. ► Effect of water-tagging of the silver complex is investigated. ► The diketo-form of the diethylmalonate complex with Au(PMe3)$^+$ preferred in the solution is also exclusively detected in the gas phase, although the enol-form should be also populated.

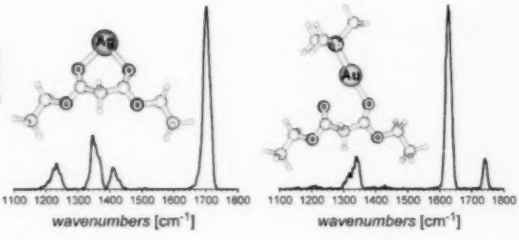

233–240

IRMPD spectroscopic and computational study of gas phase $[M(Ura\text{-}H)(Ura)]^+$ and $[M(Ura\text{-}H)(H_2O)_n]^+$ (M = Sr, Ba; n = 1, 2) complexes

Ashley A. Power, Osama Y. Ali, Michael B. Burt, Travis D. Fridgen

► The structures of $[Sr(Ura\text{-}H)(Ura)]^+$ and $[Ba(Ura\text{-}H)(Ura)]^+$ were investigated using IRMPD spectroscopy and are found to be similar to that found for $[Pb(Ura\text{-}H)(Ura)]^+$ in a previous study, except that the latter was very much non-planar due to the lone pair of electrons. ► All three species are indistinguishable in the 3200–3900 cm^{-1} region. ► Singly solvated $[Sr(Ura\text{-}H)]^+$ and $[Ba(Ura\text{-}H)]^+$ are also found to be identical to $[Pb(Ura\text{-}H)]^+$, however the doubly hydrated complexes are very different. ► All complexes are found to have a $[M(Ura\text{-}H)]^+$ core which is deprotonated at N3 and the metal is bound to N3 and O4 or to N3 and O2.

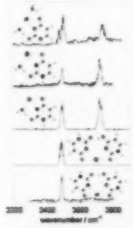

241–245

Appropriate choice of event length in sustained off-resonance irradiation collision-induced dissociation (SORI-CID) experiments: Activated ion collision-induced dissociation

Daniel N. Mortensen, Chad A. Jones, David V. Dearden

► Ion kinetic energy varies periodically during sustained off-resonance irradiation. ► Fractional SORI cycles leave kinetic energy in the system at the end of the event. ► Residual kinetic energy strongly affects the extent of ion activation.

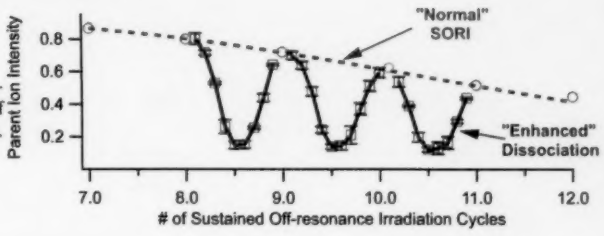

246–253

Electron induced reactions of unsaturated hydrocarbons in water clusters

K. Philip Jäger, Robert F. Höckendorf, Martin K. Beyer

► Hydrated electrons induce specific reactions in the gas phase. ► Hydrated acrylic acid radical anion initiates oligomerization of acrylic acid. ► Hydrated methyl acrylate radical anion undergoes radical addition to neutral methyl acrylate and subsequent 5-exo-trig cyclization with methanol elimination. ► Hydrated vinyl acetate radical anion undergoes cleavage of the central C–O bond. ► Cleavage of vinyl acetate radical anion strongly depends on size of hydration shell.

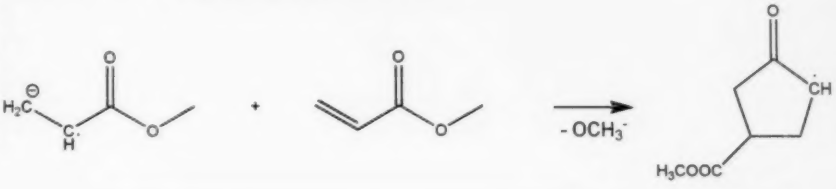

254–261

Structures of the a_2 ions of Ala-Ala-Ala and Phe-Phe-Phe

Udo H. Verkerk, Junfang Zhao, Justin Kai-Chi Lau, Tim-Wai Lam, Qiang Hao, Jeffrey D. Steill, Chi-Kit Siu, Jos Oomens, Alan C. Hopkinson, K.W. Michael Siu

► IRMPD spectra of a_2 ions of Ala-Ala-Ala and Phe-Phe-Phe are reported. ► Two isomeric a_2 ions, a cyclic imidazolidinone and a linear imine–amide, are observed, with relative abundances depending on the front end collision energy. ► DFT calculations show that the highest barrier to rearrangement of the a_2 ions is for a 1,3-proton shift across the imidazolidinone ring. ► The barrier to the 1,3-proton shift is substantially reduced by neutral solvent acting as proton shuttle.

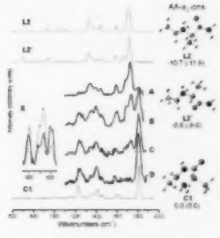

262–270

Specific and nonspecific bindings of alkaline-earth metal ions to guanine-quadruplex thrombin-binding aptamer DNA

Jongcheol Seo, Eun Sun Hong, Hye-Joo Yoon, Seung Koo Shin

► The first bindings of Sr2+ and Ba2+ to G4 TBA are specific, whereas those of Mg^{2+} and Ca^{2+} are not. ► Sr^{2+} and Ba^{2+} specifically bind to the intercalation site of G4 TBA, thereby greatly stabilizing the G4 structure. ► Mg^{2+} and Ca^{2+} nonspecifically bind to the outer region of G4 TBA. ► The second bindings of all alkaline-earth metal ions to G4 TBA are nonspecific.

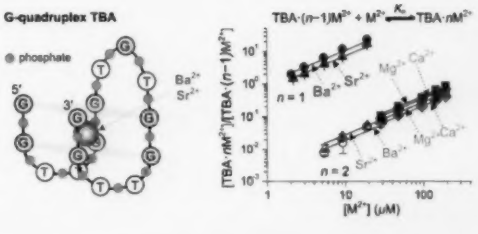

271–276

Benzene activation and H/D isotope effects in reactions of mixed cobalt platinum clusters: The influence of charge and of composition

Lars Barzen, Matthias Tombers, Christine Merkert, Joachim Hewer, Gereon Niedner-Schatteburg

► Small ionic cobalt–platinum clusters dehydrogenate benzene. ► Platinum atoms promote dehydrogenation, cobalt atoms quench it. ► Mixed triatomic clusters Co_2Pt^- and $CoPt_2^-$ show cooperative reactivity. ► Inverse kinetic H/D isotope effects prevail.

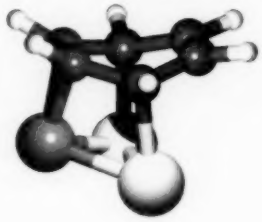

277–284

Ion transport and focal properties of an ellipsoidal electrode operated at atmospheric pressure

Zane Baird, Wen-Ping Peng, R. Graham Cooks

► Ion focusing is achieved at atmospheric pressure using an elliptical ion mirror. ► Soft landing on ambient surface achieved with ionization and transfer efficiency of 70%. ► Ambient detection of focused ions. ► Simulations adequately correspond to experimental performance.

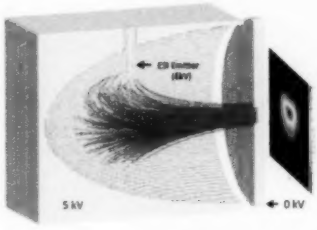

285–294

On the path to glycan conformer identification: Gas-phase study of the anomers of methyl glycosides of *N*-acetyl-D-glucosamine and *N*-acetyl-D-galactosamine

Cesar S. Contreras, Nicolas C. Polfer, Jos Oomens, Jeffrey D. Steill, Brad Bendiak, John R. Eyler

► Wavelength shifts were seen in IRMPD spectra of anomers of Li+-*N*-acetyl-D-hexosamines. ► Similar shifts were predicted using the B3LYP/6-311++G(d,p) level of theory. ► Wavelength shifts can be used for anomeric differentiation of monosaccharide epimers. ► Significant, wavelength-dependent differ-ences in IRMPD fragment ions were also seen for the isomers. ► Variable wavelength IRMPD provides another dimension for isomeric differentiation.

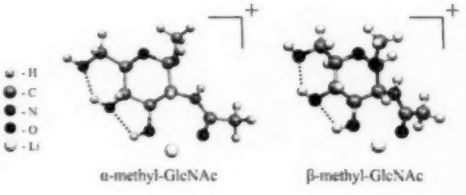

295–301

Effect of the basic residue on the energetics and dynamics of dissociation of phosphopeptides

Julia Laskin, Ricky P.W. Kong, Tao Song, Ivan K. Chu

► We examined energy and entropy effects in dissociation of protonated peptides containing phosphoserine using surface-induced dissociation combined with RRKM modeling. ► Different kinetics for H_3PO_4 loss from phosphoserine were observed under the mobile proton and nonmobile proton condition. ► The loss of H_3PO_4 from phosphoserine is a two-step process. ► In the presence of a basic residue, the phosphate abstraction from the phosphorylated side chain is followed by dissociation of the ion–molecule complex. ► The relative rate constants of the two steps determine the observed kinetics.

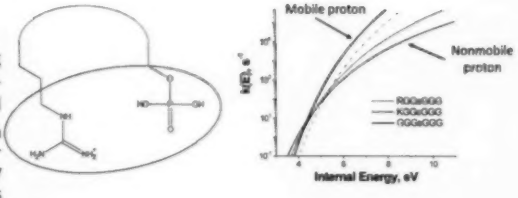

302–309

Hydrogen/deuterium exchange reflects binding of human centrin 2 to Ca^{2+} and Xeroderma pigmentosum Group C peptide: An example of EX1 kinetics

Justin B. Sperry, Zachary C. Ryan, Rajiv Kumar, Michael L. Gross

► Kinetics of H/DX of centrin 2 was measured by proteolysis and mass spectrometry. ► Kinetics shows the site of interaction of the protein with the XPC peptide. ► The kinetics constitutes an unusual example of EX1 kinetics of H/DX. ► Local unfolding of centrin/XPC gives a species that undergoes fast H/DX.